The propagation of a buoyant liquid-filled fissure from a source under constant pressure: An experimental approach

Thierry Menand, Stephen Tait

The propagation of a buoyant liquid-filled fissure from a source under constant pressure: An experimental approach

Thierry Menand
BP Institute for Multiphase Flow, University of Cambridge, Cambridge, UK

Stephen R. Tait
Department of Earth Sciences and Engineering, Imperial College of Science, Technology and Medicine, London, UK

Received 24 April 2001; revised 30 April 2002; accepted 24 June 2002; published 19 November 2002.

[1] We study the propagation of a buoyant liquid-filled fissure from a reservoir under constant pressure within the framework of linear elastic fracture mechanics. We conducted laboratory experiments by injecting aqueous solutions into gelatin solid: an analogue for elastic and brittle crustal rocks. Fissure velocity and injection rate of liquid were measured rather than being imposed. Our experimental results allow evaluation of how the different driving and resistive pressures evolved during fissure propagation and highlight the influence of the fracture resistance of the host solid. In an initial transient propagation regime, elastic pressure generated by the fissure is balanced by the fracture pressure; the fissure propagates radially with decreasing velocity and increasing injection rate, controlled by the source conditions. Subsequently, buoyancy overcomes the source pressure as the driving force, and vertical steady state propagation is established. The fissure develops a bulbous head and propagation is controlled by the balance in this head, between buoyancy pressure and fracture pressure. Even after this transition, the constant values of velocity, flux, and strain energy release rate reflect the source conditions. Our model suggests that greater horizontal dyke cross section reflects larger source pressure and that mafic dykes propagating from shallow magma chambers are unlikely to attain steady state. Moreover, our experiments place constraints on the mechanics of time-dependent failure of the solid as a process that resists fissure propagation: propagation velocity scales with the square of the height of the fissure head, and fracture toughness of rocks would be length scale dependent rather than a material property. *INDEX TERMS:* 5104 Physical Properties of Rocks: Fracture and flow; 8110 Tectonophysics: Continental tectonics—general (0905); 8145 Tectonophysics: Physics of magma and magma bodies; 8434 Volcanology: Magma migration; *KEYWORDS:* dyke, fissure propagation, analogue experiments, fracture resistance, rock failure, magma migration

Citation: Menand, T., and S. R. Tait, The propagation of a buoyant liquid-filled fissure from a source under constant pressure: An experimental approach, *J. Geophys. Res.*, *107*(B11), 2306, doi:10.1029/2001JB000589, 2002.

1. Introduction

[2] A major process of evolution of the Earth's lithosphere is the upward transport of magma by the creation and propagation of magma-filled cracks, or dykes, from zones of partially molten rocks in the upper mantle to the surface. At great depths and close to the mantellic source region magma percolates through a porous medium. Closer to the surface magma propagates by hydraulic fracturing. The latter transport mechanism is a complex problem mixing fracture mechanics, elasticity, and fluid dynamics. However, simplifications can be made: dykes may be idealized as planar sheets opening in mode I in brittle, elastic solid as the average strain associated with their emplacement, approximately their thickness to length aspect ratio, is typically of the order of 10^{-3} [*Pollard*, 1987]. Previous studies, mainly numerical, enabled us to understand separately the effects of the elasticity, the viscosity and the buoyancy of the fluid on crack propagation. Early studies presented static solutions for the equilibrium shape of fluid-filled cracks [e.g., *Pollard*, 1987]. Nevertheless, *Weertman* [1971a] showed that buoyant dykes are unstable and should move upwards. Studies that have taken into account the flow of liquid inside the fissure first focused on the coupling between elastic deformation and viscous flow and similarity solutions have been found when the injection rate is prescribed, whether the flow is laminar [*Spence and Turcotte*, 1985] or turbulent [*Emerman et al.*, 1986]. Solutions were also found for injection rates as a general power law in time [*Spence and Sharp*, 1985] and for propagation from a

0148-0227/02/2001JB000589$09.00

chamber with constant overpressure [*Spence and Sharp*, 1985; *Rubin*, 1993b, 1995a]. Subsequently, fluid buoyancy has been taken into account. *Spence et al.* [1987] and *Lister* [1990a] found solutions to the steady state case. According to *Lister* [1990a], the pressures associated with the elastic deformation and the strength of the host solid are only significant in the neighborhood of the fissure tip. The problem of the fissure shape far from its tip is thus simplified and *Spence and Turcotte* [1990] found solutions for fissures of constant volume. Similarity solutions have also been found for the lateral extent of a fissure that propagates vertically from a point source as well as its horizontal propagation in a stratified solid at the level of neutral buoyancy [*Lister*, 1990b]. *Lister and Kerr* [1991] applied these results to the propagation of magma-filled fractures and a comprehensive review of dyke propagation has been made by *Rubin* [1995b].

[3] Some experimental studies have also been carried out. However, it should be noted that few theoretical studies refer to them. All these experimental studies used a gel to simulate the elastic and brittle behavior of the Earth's crust. By injecting dyed water in gelatin, it has been shown that the direction of propagation is controlled by the stress field around the fissure which may be induced by topography [*Fiske and Jackson*, 1972] or by regional tectonics [*McGuire and Pullen*, 1989]. Further studies dealt with the effects on propagation direction of planar discontinuities in the host solid and spatial gradients in its elastic properties [*Pollard*, 1973], with formation of laccoliths [*Pollard and Johnson*, 1973; *Hyndman and Alt*, 1987], and linear elasticity has been applied to explain the shape of fluid-filled cracks in gelatin [*Maaløe*, 1987]. Following these static solutions, *Takada* [1990] seems to be the first to propose scaling laws by means of small-scale laboratory experiments. He found that fluid-filled fissures of constant volume propagate at a constant velocity which depends on the height of the fissures as well as on the difference of density between fluid and gelatin, contrary to fissures fed with a constant injection rate; in this latter case propagation velocity increases both with time and with injection rate. *Takada* [1990] also carried out experiments in which gelatin had been fractured prior to the propagation of a fluid-filled fissure. In those experiments, for which the strength of the gelatin was greatly reduced, crack velocities were observed to be two orders of magnitude greater than in experiments carried out with virgin gelatin but nonetheless were still lower by at least three orders of magnitude than velocity predicted by a Poiseuille flow, hence highlighting the role of the strength of gelatin. More recently, *Heimpel and Olson* [1994] put forward a new model for the propagation of cracks of constant volume, proposing notably that their speed might be limited by the transmission of information on the crack shape by elastic waves.

[4] Despite this intensive study we cannot answer some key questions of geological importance. For instance, what determines the flux of magma carried by a dyke? It is unlikely that a source can maintain a constant injection rate during fissure propagation. The few data on magma fluxes seem to indicate that the injection rate is not constant during the propagation of a dyke [*Brandsdóttir and Einarsson*, 1979; *Einarsson and Brandsdóttir*, 1980]. Furthermore, assuming a steady state boils down to not taking into account the initiation process. As a consequence the physical characteristics of the source are no longer linked to propagation and are excluded from the model. *Mériaux and Jaupart* [1998] studied crack propagation from a reservoir under constant overpressure and showed that the initial crack loading determines its subsequent propagation. However, these authors, like others, have neglected the fracture resistance of the solid. This was mainly motivated by laboratory measurements on rock samples [e.g., *Atkinson*, 1984]. Based on scaling analysis, it is shown that once a dyke has been initiated and has grown to a critical length, the pressure associated with the strength of rocks is negligible in comparison with the other pressure scales, especially magma viscous resistance [*Lister*, 1990b; *Lister and Kerr*, 1991]. However, field estimations give values 10^2-10^3 times greater than those measured in the laboratory [*Delaney and Pollard*, 1981; *Reches and Fink*, 1988]. Moreover, it is difficult to believe that fracturing is negligible from the very beginning of the propagation in the case of flawless solids. Hence we ask, how may a dyke grow from a regime where the fracture resistance of rocks would be significant to a regime where it could be neglected?

[5] We suppose in our study that magma cannot intrude the surrounding rock by hydraulic fracturing as long as the fracture resistance of the rock is not overcome. Similar to most studies on dyke propagation we base our analysis on linear elastic fracture mechanics. Therefore, we assume that a liquid-filled crack cannot propagate as long as the stress intensity factor K at its tip does not reach the fracture toughness K_c of the surrounding solid. One basic question is whether K_c is a material property independent of the crack dimensions and loading. This has been assumed in the vast majority of the literature on dykes, although *Rubin* [1993a] has argued that this vision may not be adequate for dykes at high confining pressure. We use this simplification in our initial approach but will return to this key issue in the light of our experimental results. We do not deal with the influence of the volatiles that could be present at the crack tip [*Barenblatt*, 1962]. A theoretical investigation of this effect has been made by *Lister* [1990a] and the hypothesis that such volatiles could be an origin for precursor volcanic eruptions has been experimentally investigated by *Menand and Tait* [2001]. Finally, because we concentrate on the mechanical aspects of the problem, we do not take into account thermal effects.

[6] Fracturing processes are very difficult to handle in numerical models whereas they are always present in laboratory experiments using gelatin [*Takada*, 1990; *Lister and Kerr*, 1991]. In this paper, we study with laboratory experiments the propagation of a fissure fed by a reservoir under a constant pressure. In these experiments, aqueous solutions are injected in gelatin solids simulating the elastic, brittle crust and care was taken to start fissure propagation from a well-characterized initial condition. We first introduce the experimental techniques that we developed to measure in situ Young's modulus and the fracture toughness of gelatin solids with which we characterize their rheology. We then present our experiments and propound a new model of fluid-filled fissure propagation. We conclude with a short discussion on our

results and the geological application and implications of our work.

2. Rheology of the Gelatin

[7] Gelatin is a clear, brittle, viscoelastic solid with a low shear modulus and a Poisson's ratio of nearly 0.5. It has been used in experimental studies of dyke propagation because its low shear modulus allows it to deform significantly under gravity at laboratory scale [e.g., *Fiske and Jackson*, 1972; *Maaløe*, 1987; *Takada*, 1990; *Heimpel and Olson*, 1994]. If it was assumed in these studies that gelatin behaves in an elastic, brittle manner, such an assumption however has never been carefully verified. Elasticity and brittleness are two different properties. However, *Griffith* [1920] and *Irwin* [1957] showed that they are not independent for elastic solids. In this ideal case, fracture toughness follows the relation

$$K_c = \sqrt{2\,\gamma_s\,E}, \tag{1}$$

where E is the Young's modulus of the elastic solid and γ_s is its surface energy which is thought to depend only on the temperature [*Griffith*, 1920]. Elastic solids of a similar composition at a given temperature should have surface energies of the same order of magnitude and therefore should differ only by their Young's modulus. We thus developed techniques to measure Young's modulus E and fracture toughness K_c of gelatin solids in situ in our experiments, which allowed us to verify relation (1) for gelatin.

[8] High-clarity, 200 bloom, acid, pigskin-derived gelatin in granular form was supplied by SKW Bio-Systems. The gelatin was prepared by dissolving the powder in distilled water. The solution was heated until complete dissolution of the gelatin at 60°C, after which 0.1% sodium hypochlorite was added to prevent fungal growth. The gelatin was then poured in two identical acrylic tanks; one to measure its Young's modulus and the other to measure its fracture toughness. The gelatin was left to solidify in these two tanks under hydrostatic conditions, horizontal strains are nil and Poisson's ratio $\nu = 0.5$, in an air-conditioned room at 20°C for 48 hours, timescale of gelification was approximately 1 day for the concentrations used, in order to ensure thermally homogeneous gelatin solids. A thin layer of silicon oil was poured on the gelatin surface in order to avoid evaporation during solidification, which would create a gradient of gelatin properties. Once the gelatin was solid both measurements of E and K_c were performed.

2.1. The Measurement of Young's Modulus

[9] We measured Young's modulus of the gelatin solid by putting a rigid, circular cylinder, made of duraluminum, on the surface of the gelatin. The radius of this object was small compared to the dimensions of the tank; the gelatin could thus be seen as a semiinfinite medium. The vertical deflection w created was then measured and Young's modulus was calculated by means of the following relation [*Timoshenko and Goodier*, 1970]:

$$E = \frac{M\,g\,(1-\nu^2)}{2\,a\,w}, \tag{2}$$

where M and a are the mass and radius of the cylindrical weight, g is the gravitational acceleration, and ν is the Poisson's ratio of the gelatin. The crucial point is to measure the deflection as accurately as possible. This was done by using a digital micrometer to determine the position of the top of the weight with respect to a reference position rigidly attached to the tank. This method allowed us to measure E with an error less than 2.5%. Solids of different Young's modulus were made by changing the concentration of gelatin. Note, however, that Young's modulus of a gelatin is not a constant but continuously increases with time as gelification continues. Thus, for each experiment, several measurements of Young's modulus were made and the experiment was carried out when the desired value of E was attained. Experimental durations were less than 5 min, a short time period when compared to the time evolution of Young's Modulus so it could be assumed to be constant during an experiment.

2.2. The Determination of the Fracture Toughness

[10] In the case of an edge crack embedded in a semiinfinite elastic solid, the stress intensity factor K at the crack tip may be expressed as [*Sneddon and Das*, 1971]

$$K = \alpha\,\overline{\Delta P}\,\sqrt{\pi\,h}, \tag{3}$$

$\overline{\Delta P}$ being the overpressure of the crack averaged over its height h. The overpressure of the crack is defined as the difference between the pressure in the crack and the stress in the solid in the absence of the crack. α is a dimensionless factor which is a function of boundary conditions, especially those at the surface of the semiinfinite solid, in the case of a crack embedded in an infinite elastic solid we would have $\alpha = 1$.

[11] We created a small edge crack in our gelatin by plunging a rigid, metallic blade, made of stainless steel, in the solution of gelatin before its solidification. Once the gelatin was solid, the blade was carefully removed. The fissure was then filled with water as well as the part of the tank that was free of gelatin. The tank was then turned over in order to have the water reservoir beneath the gelatin and the reservoir was fed in such a way that its pressure balanced exactly the weight of the gelatin. According to linear elastic fracture mechanics, once the stress intensity factor K at the tip of the fracture reaches the fracture toughness K_c of the solid the crack propagates. This was achieved by slowly increasing the crack overpressure: we injected some air into the crack by using compressed air going first through a pressure reducer and then through a small capillary positioned in the fissure. As air was injected into the crack, the excess water was bled from the reservoir in order to maintain a free surface condition at the interface between the reservoir and the gelatin. The experimental apparatus is schematically drawn in Figure 1. Measuring the height of air in the fissure, which gives us the crack overpressure at the onset of its propagation, and using equation (3) we calculated the stress intensity factor at the crack tip. The calculation requires determination of the factor α, which was done following the work of *Sneddon and Das* [1971] for an edge crack linked to a free boundary. We identified this

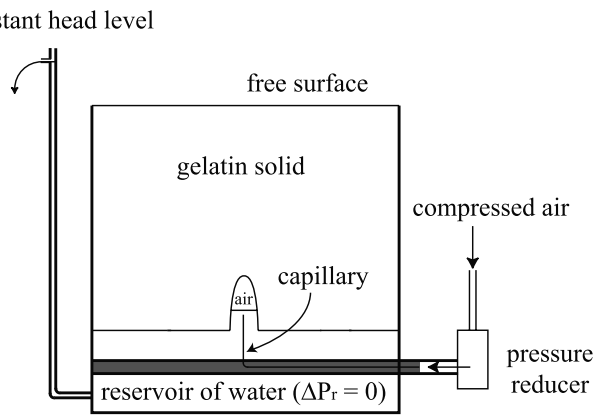

Figure 1. Schematic diagram of the experimental apparatus used for the determination of the gelatin fracture toughness. The excess of water is bled off the reservoir while air is injected in the crack insuring a free surface condition at the interface between the water reservoir and the gelatin solid.

stress intensity factor with the fracture toughness of the gelatin solid.

2.3. Relationship Between Young's Modulus and Fracture Toughness

[12] In the case of an edge crack embedded in a semi-infinite elastic solid, the stress intensity factor at the crack tip differs from the case of a crack in an infinite elastic solid by the factor α. However, we can still apply the approaches developed by *Griffith* [1920] and *Irwin* [1957]. Therefore, if our gelatin solids behave in a pure elastic manner they should obey relation (1). Figure 2 is a plot of K_c of our different gelatin solids as a function of their Young's modulus. The plain curve corresponds to the theoretical equation (1). The best fit through our data is

$$K_{c\,\mathrm{exp}} = 0.97\,E^{0.55}\ \mathrm{Pa\ m^{\frac{1}{2}}}. \tag{4}$$

Taking into account the error bars on K_c and E our data are in good agreement with the expected theoretical relation for pure elastic, brittle behavior. Furthermore, equation (4) enables us to calculate the fracture toughness of a gelatin solid from the measurement of its Young's modulus, the obvious advantage being the nondestructive determination of the latter. It also gives us the surface energy of the gelatin solids: $\gamma_s \simeq 1\ \mathrm{J\ m^{-2}}$.

3. Propagation of a Buoyant Fissure From a Reservoir Under Constant Overpressure

3.1. Experimental Method

[13] In this section we present the experimental apparatus that we used to study the propagation of a water-filled fissure from a reservoir under constant overpressure (Figure 3). Details of experimental conditions are given in Table 1. Gelatin was set under hydrostatic conditions in an acrylic tank 30 cm wide by 50 cm high. A rigid reservoir filled with dyed water was situated beneath the gelatin tank. The injection of water into the gelatin was allowed by a 5 mm wide and 20 cm long slit made in the undeformable roof of the reservoir. Furthermore, the reservoir was fed by an additional reservoir placed on a small elevator. This elevator enabled us to lift the additional reservoir in order to increase the reservoir overpressure. Once the small elevator was locked, the additional reservoir fed the main reservoir with a given head level. This header tank was large enough to maintain a constant head level during the propagation because the total volume of water injected in a crack was small, the maximum variation of the head level was 1–2 mm. Therefore the reservoir overpressure stayed constant during the crack propagation. We also measured the injection rate using scales placed on the small elevator and beneath the additional reservoir. The scales were linked to a PC, which recorded the mass of water lost by the reservoir and thus injected into the crack. This allowed us to measure the injection rate instead of imposing it. The propagation was videotaped in order to measure the crack tip velocity. The video camera was manually moved up on a vertical track to keep it level with the tip of the fissure.

[14] Inside the reservoir was a movable plate on which a 1 mm thick, 1.5 cm high, and 12 cm long metallic blade, made of stainless steel, was mounted. Before pouring the gelatin solution into its tank, we initially sealed the slit with the movable plate. This way, the metallic blade penetrated the slit in the reservoir roof. Once the gelatin was solid, the plate was carefully moved down. The metallic blade was thus taken out of the gelatin solid and created a small fissure filled with fluid from the reservoir. This technique enabled us to propagate the fissure from a well characterized linear source.

[15] Just prior to starting an experiment, the Young's modulus of the gelatin was measured by the technique described in section 2.1. The reservoir overpressure, initially nil, was slowly increased with the aid of the small elevator and the head level was maintained constant once the fissure started to propagate. The injection rate was then recorded and the propagation was videotaped.

3.2. Experimental Observations and Measurements

[16] When the fissure started to propagate, we observed in all experiments that the propagation was initiated from a

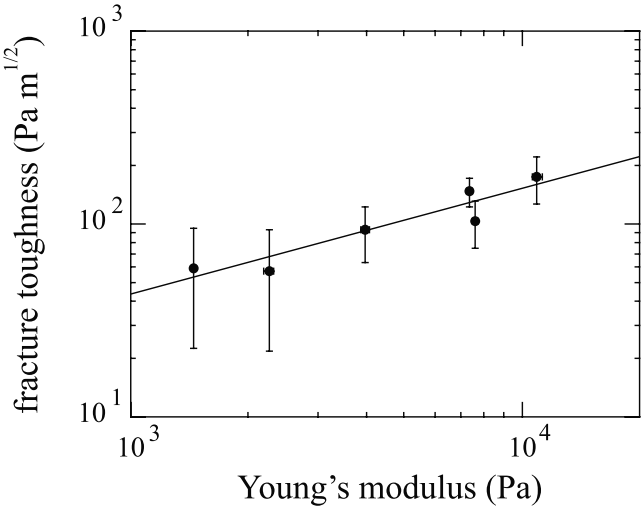

Figure 2. The fracture toughness K_c as a function of the Young's modulus E for different gelatin solids. Each point represents a gelatin solid. The plain curve represents the theoretical equation $K_c \propto \sqrt{E}$.

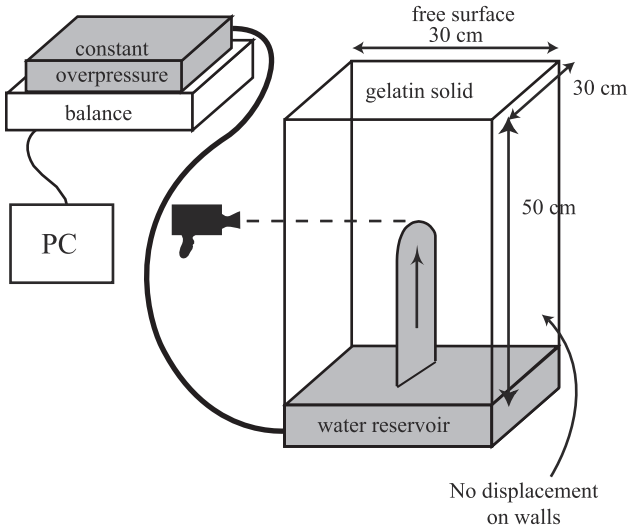

Figure 3. Schematic diagram of the experimental apparatus used for the propagation of a water-filled fissure from a reservoir under constant overpressure.

point of the linear source. Then, the source injection extended laterally and the fissure propagated radially in a nearly vertical plane. We also observed that the fissure had an approximately elliptical cross section, as expected for a pressurized cavity embedded in an elastic solid [*Sneddon*, 1946]. The form of the fissure during this early stage of the propagation is shown on Figure 4. Afterward, the propagation became mainly vertical and the shape of the fissure stretched out vertically. Moreover the fissure seemed to develop a head thicker than its tail. This was not easily observed because the fissure sometimes became slightly curved and was not along the axis of the camera, but it was particularly noted in experiments 19, 20, and 22. The transition between the initially radial and later vertical propagation occurred after typically 10–15 cm of propagation. Figure 5 shows the shape of the fissure after the transition. In almost all experiments we observed that during propagation in the uppermost part of the tank, after approximately 25–30 cm of propagation, the fissure deviated from vertical trajectory and followed a path that curved toward one side of the tank, presumably due to wall effects. We will restrict our description to the part of the fissure propagation, which is not affected by the walls of the tank.

[17] We measured the distance of propagation of the fissure and the mass of water injected into the fissure as functions of time, as shown on Figure 6 for experiment 24. Instantaneous velocity was calculated by differentiating a linear regression through the distance data for five fissure positions, the point on which the fit was centered and two either side. The instantaneous volumetric injection rate was calculated in the same manner from the mass data divided by the density of the fluid. Figure 7 is a plot of the velocity and the injection rate of the fissure as a function of its length for experiment 24, deduced from the data shown on Figure 6. The velocity data seem to be noisier than the injection rate data. This may be due to the measurement procedure that we used, the video camera was manually moved up, although we cannot rule out that this effect may be real and related to the dynamics of propagation. However, there are clearly two different regimes. This is particularly visible from the injection rate data, the transition between the two regimes occurring after about 10 cm of propagation in this case, experiment 24. The first regime was characterized by an increasing injection rate and a decreasing velocity. This implies that the fissure inflated and/or propagated laterally at the level of the source. It seems therefore that there is a correspondence between these velocity and injection rate measurements and the radial propagation we initially observed in the experiments. In the second regime, both the fissure velocity and the injection rate were essentially constant. This steady state was not imposed in our experiments but rather was naturally adopted by the system; we emphasize that this steady state was approached from a regime with an increasing flux and a decreasing velocity.

[18] Finally, in all experiments the flow inside the fissure was always laminar. In the case of a fissure of width w, which is filled with a liquid of density ρ and viscosity η, and that propagates at a velocity u, flow inside the fissure is turbulent if the Reynolds number $R_e = \frac{\rho u w}{\eta}$ exceeds a critical value of order 1000. Conversely, flow is laminar if $R_e \leq 1000$. In all experiments, the injected liquid was water, for which density and viscosity are 1000 kg m^{-3} and 10^{-3} Pa s, respectively, the velocity of propagation was always less than 1 cm s^{-1} and the fissure width was always less than 5 mm. As a consequence, the Reynolds number R_e was always less than 50.

3.3. The Different Pressure Scales

[19] In order to quantitatively analyze our observations, we follow *Lister* [1990b] and *Lister and Kerr* [1991] and define five different pressure scales. The geometry of the fissure that we use is shown on Figure 8. The height of the fissure is h, its breadth is $2b$, its thickness is $2w$ and we use the letter l when we refer to a length, h or $2b$, in a nonexplicit manner. There are three driving pressures. These are the elastic pressure scale required to open the fissure

$$P_e \sim \frac{E}{2(1-\nu^2)}\frac{w}{l}, \tag{5}$$

where l is the smallest of the height or the breadth of the fissure, the source overpressure ΔP_r and the hydrostatic, or buoyancy, pressure

$$P_h \sim \Delta\rho\, g\, h, \tag{6}$$

where $\Delta\rho$ is the difference between the density of the solid and the density of the liquid, so that the fluid overpressure is

Table 1. Details of the Experimental Conditions[a]

Experiment	ρ_g (kg m^{-3})	ρ_l (kg m^{-3})	η (Pa s)	E (Pa)	ΔP_r (Pa)
19[b]	1013.0	1000.6	10^{-3}	1525	749
20	1013.0	1000.0	10^{-3}	1581	327
21	1013.0	1000.3	10^{-3}	929	190
22	1024.9	1001.2	10^{-3}	5529	749
24	1024.6	1001.2	10^{-3}	7899	1133

[a] All experiments were dyed water injected in gelatin solid. ΔP_r corresponds to the reservoir overpressure needed to propagate the fissure. The overpressure was progressively increased until the fissure propagates except in experiment 19: ΔP_r has violently been imposed and fissure has immediately propagated.

[b] ΔP_r violently imposed.

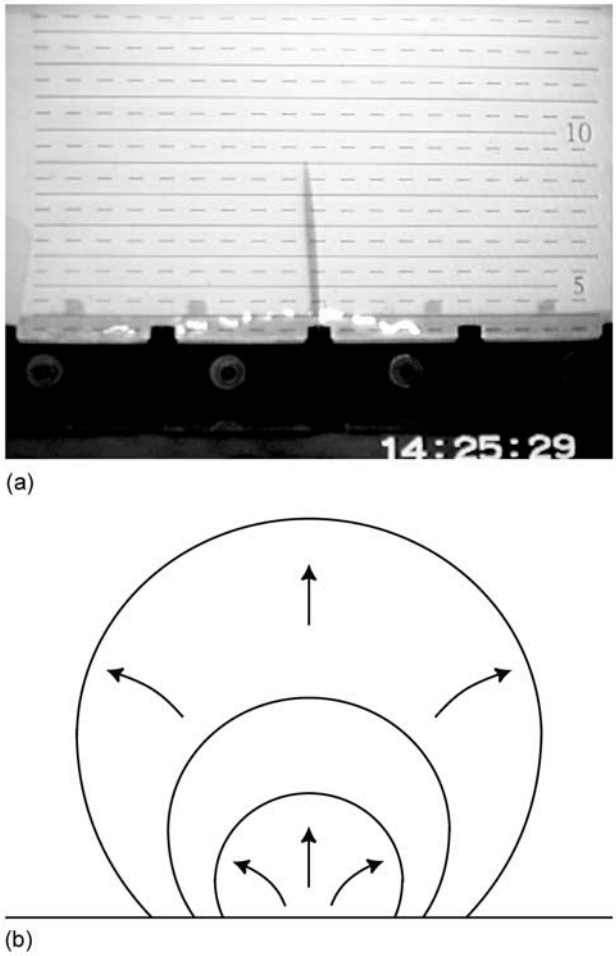

Figure 4. The shape of the fissure during the early stage of its propagation in experiment 22. The photo (a) taken after 9 cm of propagation shows the elliptical cross section of the fissure. The in plane view (b) is a schematic illustration of the radial propagation.

the sum of ΔP_r and P_h. The two other scales are resistive pressures. One is the viscous pressure drop

$$P_v \sim \frac{3\,\eta\,u\,l}{w^2}, \tag{7}$$

where η is the viscosity of the fluid, u the average velocity of the fluid inside the fissure, which is also the fissure velocity, and l the length of the fissure. The other is the fracture pressure

$$P_f \sim \frac{K}{\sqrt{\pi\,l}}. \tag{8}$$

This is the overpressure needed by the liquid to generate a stress intensity factor K at the crack tip, which should be at least equal to K_c for the host solid to be fractured.

[20] The elastic pressure (5) and the fracture pressure (8) are quasi-static from an elastic point of view, which means that they are not necessary valid for the dynamic problem of the propagation of a fissure. However, the use of these equations in the present study is justified by the fact that fissures propagated with velocities that were two orders of magnitude less than the velocities of elastic waves, hence propagated quasi-statically: in the range of the experimental conditions, shear wave velocities were approximately

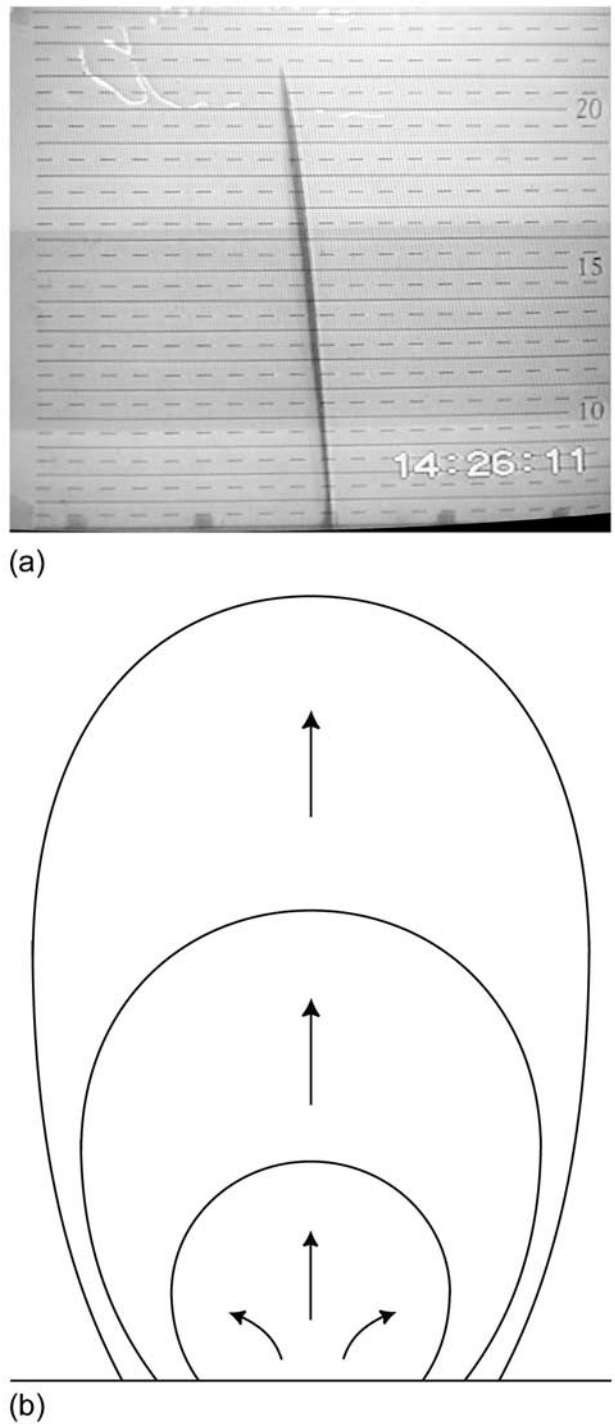

Figure 5. The shape of the fissure in cross section, in experiment 22, after 21 cm of propagation (a). The fissure seemed to develop a head thicker than its tail. Initially radial, the propagation became mainly vertical as schematically illustrated by the in plane diagram (b).

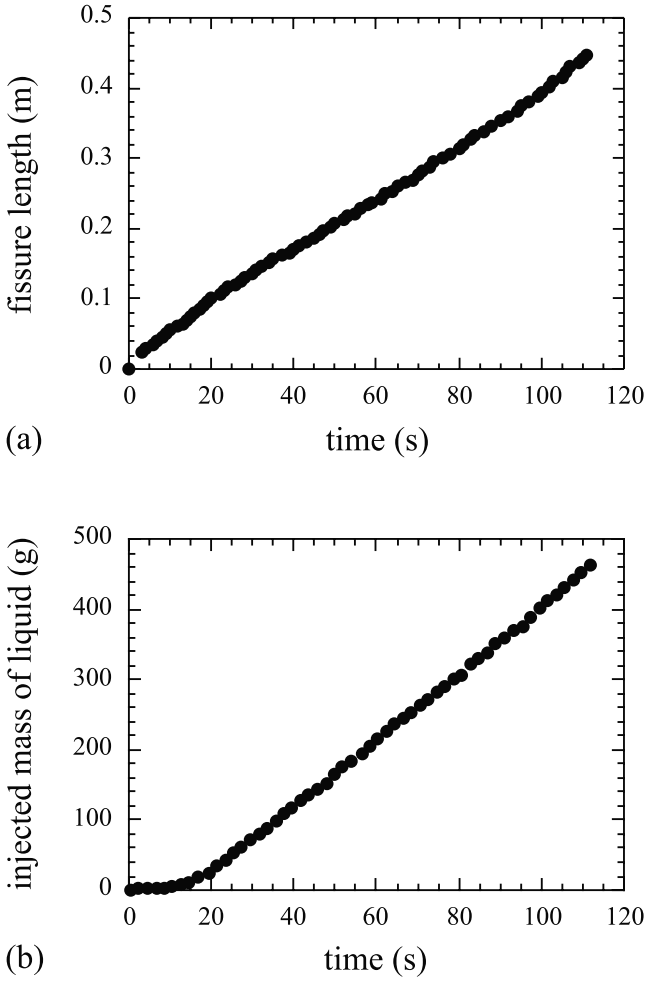

Figure 6. The distance of propagation of the fissure (a) and the mass of water injected in the fissure (b) as a function of time in experiment 24.

equal to 1 m s^{-1} while fissure velocities were always less than 1 cm s^{-1}.

3.4. Initial Propagation Regime

[21] We initially observed that the propagation was radial and in a vertical plane or nearly so, in short, there was no specific direction for fissure propagation. This suggests that the buoyancy pressure (6) was initially negligible compared with the other pressure scales. The initial height of the fissure was indeed small, 1.5 cm. Moreover, the fissure velocity was low as well as the viscosity of the injected liquid, water for which $\eta = 10^{-3}$ Pa s, suggesting that the viscous pressure drop (7) could be neglected as well.

[22] This can be shown quantitatively by comparing terms explicitly. The fissure was observed to have an ellipsoidal shape and to resemble "half a penny" so that its breadth was approximately equal to twice its height. Its basal width, $2w$, is thus easily expressed as a function of its volume V, which is known from the data of the mass of injected fluid:

$$2w = \frac{3V}{\pi l^2}. \tag{9}$$

It appears that, except in experiment 24, the basal width of the fissure remains nearly constant, influenced by the lower boundary condition of no displacement on the lower gelatin surface, as expected. In experiment 24, however, the fissure width appears to be proportional to the fissure length implying that the elastic pressure remains constant, as would be expected if slip occurred between the base of gelatin solid and the base of the tank. We assume that in this case, the gelatin adhered less well to the tank base than in the other experiments, although we were unable to check it independently. Equation (9) enables us to express the pressure scales as functions of V rather than w. Figure 9 represents the evolution of the four pressure scales (5)–(8) during the fissure propagation for the two boundary conditions: no displacement and slip displacements. It shows that the buoyancy pressure and the viscous pressure drop can be neglected during the initial propagation regime in both cases. Note that, in this transient regime, the viscous pressure drop stayed constant in most experiments and even decreased in the slip displacement case. This suggests that, initially, propagation occurred in a regime characterized by an approximate

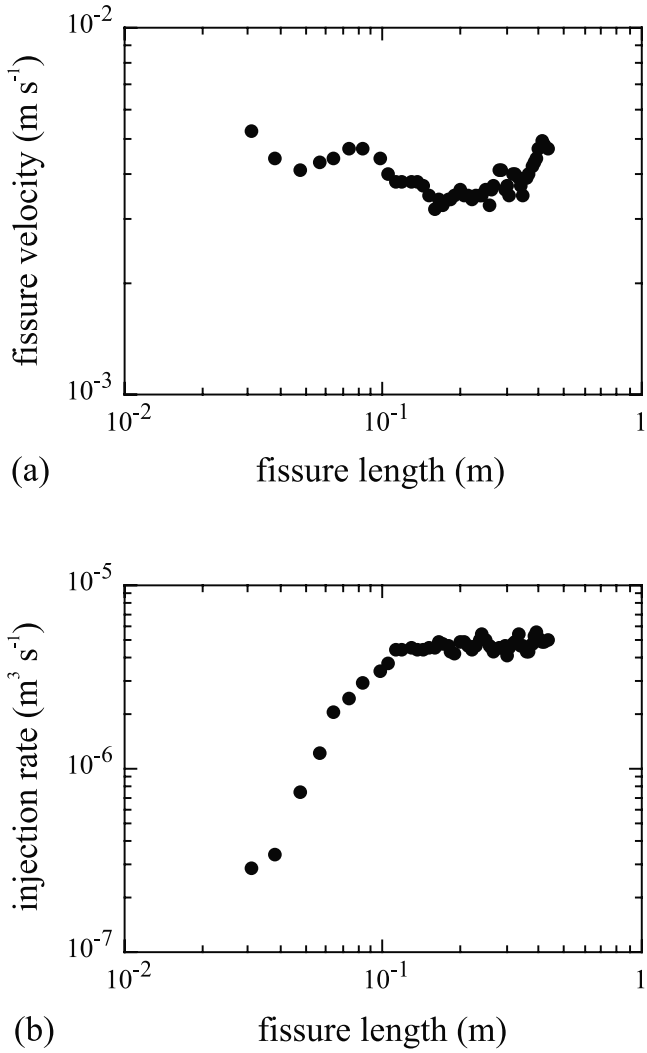

Figure 7. The velocity (a) and the injection rate (b) of the fissure as a function of its length in experiment 24.

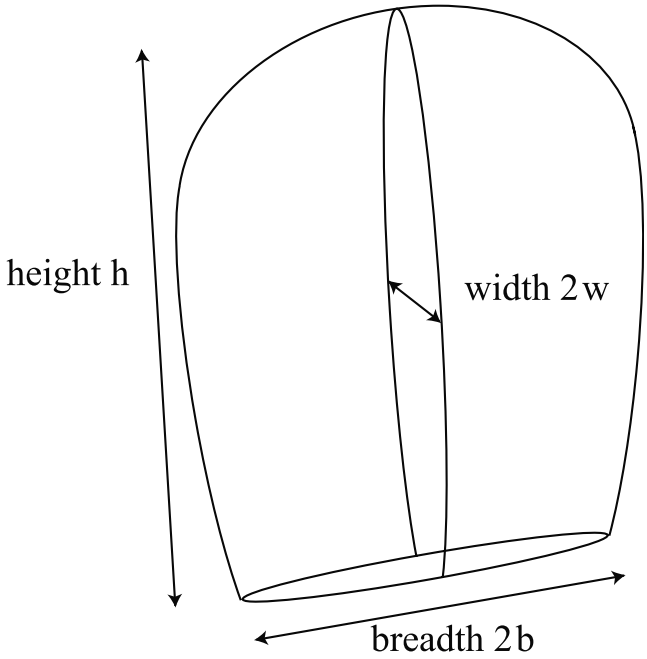

Figure 8. Schematic diagram of a fissure. The fissure has a height h, a breadth $2b$, and a thickness $2w$ such as $2w \ll 2b \leq h$.

balance between the elastic pressure (5) and the fracture pressure (8); as propagation was quasi-static, dilation of the fissure occurred much faster than propagation and during this initial regime the elastic pressure balanced the source overpressure while propagation was controlled by the stress intensity factor at the tip of the fissure:

$$\frac{E}{2(1-\nu^2)}\frac{w}{l} \sim \Delta P_r \sim \frac{K}{\sqrt{\pi l}}. \tag{10}$$

[23] The quasi-static behavior of the fissure is not assumed but observed. The volume of the fissure V is function of the constant fissure width (equation (9)). By differentiating it with respect to time and dividing by the velocity $u = dl/dt$, we obtain the ratio of the flux $q = dV/dt$ over the crack velocity u as a linear function of the crack length. In experiment 24 however the elastic pressure rather than the fissure width was constant and V must be expressed as a function of the constant overpressure in the fissure ΔP_r before differentiating it with respect to time, by combining equations (9) and (10). We therefore obtain that

$$\frac{q}{u} = \beta\frac{V}{l}, \tag{11}$$

with the numerical factor $\beta = 2$ for experiments 19–22 and $\beta = 3$ for experiment 24. Figure 10 shows that the experimentally measured ratios q/u follow the quasi-static relation (11).

[24] We therefore have observational evidence that the fissure is behaving quasi-statically, from an elastic point of view, even though it is propagating and even though the stress intensity factor at its tip K is larger than the fracture toughness K_c, as suggested by equation (10). Moreover, equation (10) implies that the rate of propagation of the fissure was being controlled in some way by time-dependent failure of the solid ahead of the tip. Before discussing the implications of this idea for dyke propagation we describe the propagation observed during the latter stages of experiments.

3.5. Steady State Regime

[25] After 10–15 cm of propagation we observed a new regime characterized by a constant fissure velocity and a constant injection rate. Furthermore, we observed that the propagation became mainly vertical which suggests that the buoyancy pressure had become an important driving force. Indeed, according to Figure 9, the buoyancy pressure P_h becomes comparable to the elastic pressure P_e at approximately this height. As the fissure propagated, the buoyancy

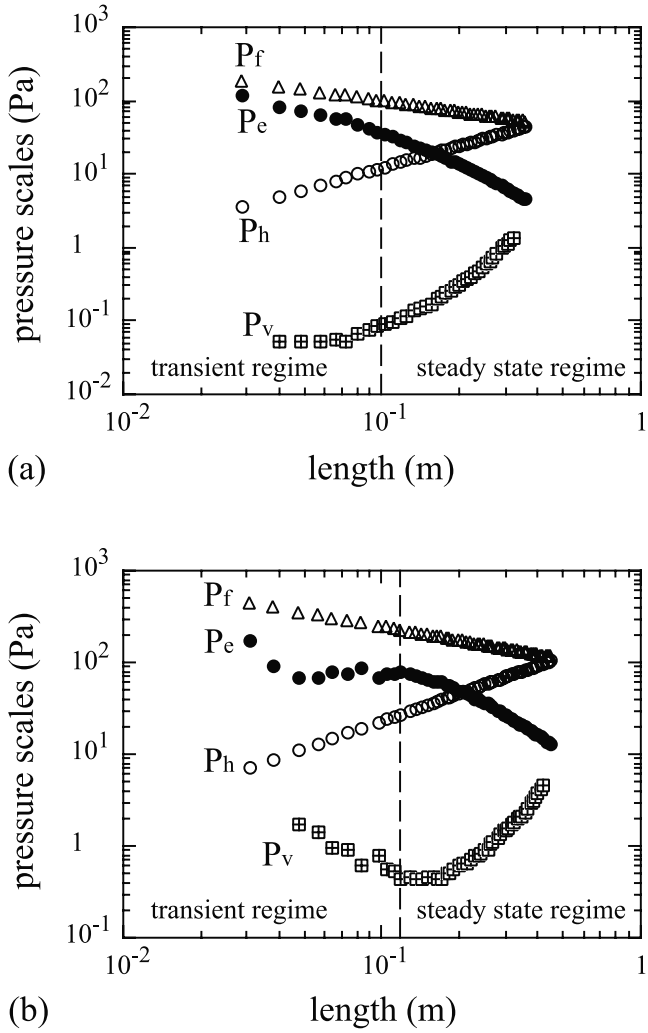

Figure 9. The evolution of the four pressure scales during the fissure propagation for two different lower boundary conditions: (a) no displacement, experiment 19 in the present case, and (b) slip displacements, experiment 24. In both cases, the stress intensity factor at tip of the fissure has been assumed to be equal to the fracture toughness of the solid during the whole propagation. The vertical dashed line separates the transient initial regime from the steady state one, as observed from the velocity and injection rate data.

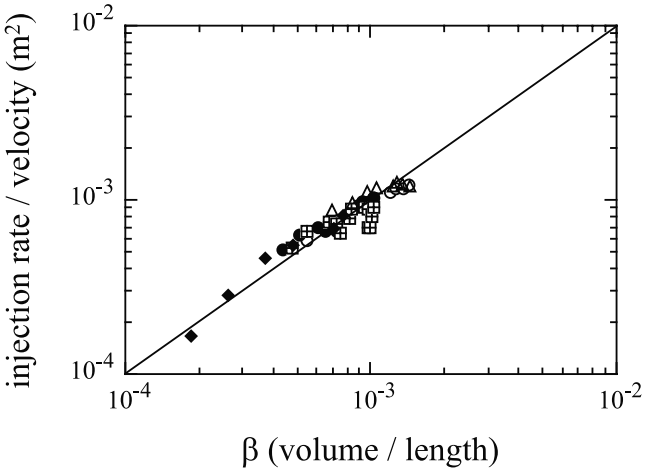

Figure 10. The ratio of the volumetric injection rate q over the crack velocity u as a function of the ratio of the volume of the fissure V over its length l. $\beta = 2$ for experiments 19–22 and $\beta = 3$ for experiment 24 in order to compare all the data on the same graph (see text). Each symbol represents an experiment: ○ 19, ● 20, ⊞ 21, △ 22, and ◆ 24. The plain curve is the theoretical relation $\frac{q}{u} = \beta \frac{V}{l}$.

increased. Ultimately, when the fissure reached a critical height

$$l_c \sim \frac{\Delta P_r}{\Delta \rho g}, \tag{12}$$

the buoyancy pressure and the fissure overpressure were of the same order. Moreover, the viscous pressure drop P_v was negligible in comparison to the fracture pressure (Figure 9). It is therefore reasonable to assume that propagation was controlled subsequently by a balance between P_h and P_f:

$$\Delta \rho g l_c \sim \frac{K}{\sqrt{\pi l_c}}. \tag{13}$$

This new balance explains the transition from a radial to a vertical propagation. We also observed qualitatively that the fissure developed a bulbous head although this was not practically possible to quantify. We propose that once the buoyancy pressure overcame the source pressure, the fissure developed a bulbous head of length l_c (equation (12)) that was connected to the source by a thinner tail and that the propagation was controlled by the balance which took place in this head between the buoyancy pressure and the fracture pressure. Figure 11 is a schematic illustration of such a propagation. At this point, the fissure head, in which elastic and buoyancy pressures are in balance, had a thickness

$$w_c \sim \frac{2(1-\nu^2)}{E} \Delta P_r l_c \sim \frac{2(1-\nu^2)}{E} \frac{\Delta P_r^2}{\Delta \rho g}. \tag{14}$$

The fissure tail was thinner and viscous pressure drop is expected to be important there. Figure 9 shows that, in the steady state regime, it increased linearly with the height of the tail. So did the buoyancy pressure. Our interpretation is that the buoyancy balanced exactly the viscous pressure gradient as the tail of the fissure steadily lengthened and adjusted elastically its thickness w_s in order to maintain such a balance. According to *White* [1974], this thickness was

$$w_s = \left(\frac{4 \eta q}{\pi b \Delta \rho g} \right)^{\frac{1}{3}}, \tag{15}$$

where b is half the breadth of the fissure tail.

[26] At the transition between regimes, when the fissure had a height l_c, the buoyancy pressure generated a stress intensity factor K_t at the tip of the bulbous head. At the transition, both balances (10) and (13) should be approximately valid. By combining these two equations with the ratio q/u, used as a kinematic estimate for the cross-sectional area of the fissure $\pi w l_c$, we obtain that

$$l_c \sim \left[\frac{E}{2(1-\nu^2)\pi \Delta \rho g} \frac{q}{u} \right]^{\frac{1}{3}}, \tag{16}$$

and

$$K_t \sim \left[\frac{E \Delta \rho g}{2(1-\nu^2)} \frac{q}{u} \right]^{\frac{1}{2}}. \tag{17}$$

There is therefore a correspondence between a constant stress intensity factor at the fissure tip, which controls the fissure propagation, and the observed steady state propagation, with a constant ratio q/u. We propose that the steady state propagation was established by the constant head height l_c, and therefore the constant stress intensity factor K_t, that was determined at the transition between regimes. In this interpretation, the tail fed in a passive manner the steadily propagating fissure while the buoyancy pressure in its head overcame the fracture pressure and we suppose that the fracturing processes that controlled the propagation operated in a quasi-static manner.

4. Discussion

4.1. Results

[27] We have found that a buoyant liquid-filled crack fed by a reservoir under constant pressure can steadily propagate. The shape of the fissure in the steady state regime was the same as in the "viscous model [*Lister and Kerr*, 1991]." In fact, once the steady state regime is achieved, the head regime that we describe and the tail regime of the "viscous model" are exactly balanced, and hence we cannot tell the difference in a sense. That our model, controlled by fracture resistance of the host solid, and the "viscous model" give identical steady state regimes might seem a paradox. It is not: we show that we must take account of the transient regime through which the steady state is approached in order to know what the steady state will be. The "viscous model" determines what shape of crack is required to satisfy the assumed steady state propagation. This assumption means that the source is excluded, and thus we lose important information: we cannot say what kind of a geological source we are dealing with, at least not more than that it must be able to maintain a constant flux. We should therefore expect that in this steady state framework, the fracture toughness does not affect the rate of propagation, as the "viscous model" indeed shows.

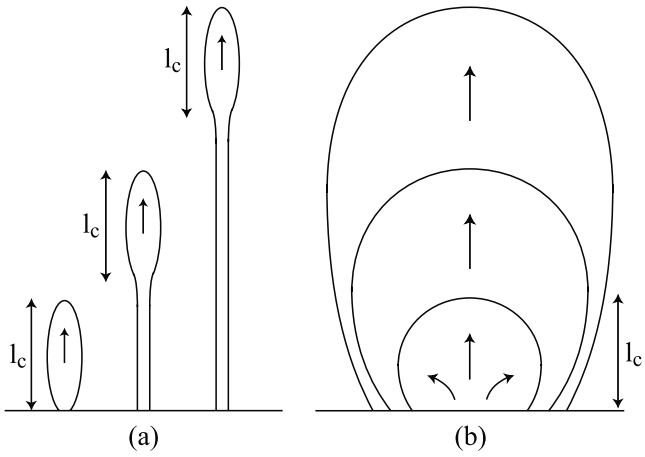

Figure 11. Schematic illustration of the fissure propagation in the steady state regime in cross section (a) and in plane (b) views. Once the fissure reaches a height l_c, the hydrostatic pressure and the source pressure become comparable. Then, the fissure propagates mainly vertically and develops a bulbous head of length l_c. The propagation is controlled by the balance that takes place in the fissure head between the hydrostatic pressure and the fracture pressure.

[28] But this vision is too restrictive. At steady state the head and the tail must have the same speed, but different physical balances determine their respective velocities. We show that if the source is characterized by relatively constant pressure, which is reasonable physically, the speed of propagation in fact initially depends on the pressure in the source and the fracture toughness (Figure 9) and this also determines the speed of the head in the subsequent steady state. Once a dyke has reached a buoyancy-driven steady state, although the source is no longer directly "visible" (i.e., as in the "viscous regime"), the source is "remembered" in the following sense. The flux and velocity of the dyke transiently adjust in the fracturing regime to the steady state that is consistent with the source pressure and the fracture characteristics of the host as well as the density and viscosity of the liquid. Hence it is important geologically to characterize as well as possible this fracturing regime that we have shown to exist.

[29] However, the way fracturing processes operate at the fissure tip remains unclear. In our experiments, the viscosity of the liquid appears to exert no active control on the velocity of crack propagation. Propagation is controlled by time-dependent failure of the gelatin solid at the tip of the crack. The linear elastic fracture mechanics framework does not contain any timescale and thus cannot provide a model for propagation velocity; it only provides a threshold above which the solid fractures and thus crack propagation takes place. Nevertheless, our experiments provide some constraints on failure-controlled crack propagation. In the case of buoyant liquid-filled cracks of constant volume, it has been argued that, all else being equal, the velocity of cracks should be proportional to the square of their height [*Heimpel and Olson*, 1994, equation (8)]. Recently, it has been observed that fissures that have a growing gas pocket at their tip propagate with velocities proportional to the square of the height of the gas pocket, which is the fissure head [*Menand and Tait*, 2001]. There is no conceptual difference between this study and the steady state regime observed in our experiments; the tail of gas driven fissures does not play any role in the propagation, the latter being entirely controlled by the fissure head. We should therefore find that our fissures and those driven by gas are subject to the same fundamental control. Figure 12 shows that velocity data from both sets of experiments can indeed be correlated:

$$u \propto \Delta\rho\, l_c^2. \tag{18}$$

This relationship highlights that as l_c was determined by the source conditions, $l_c \sim \Delta P_r/(\Delta\rho g)$ and $\Delta P_r \sim K_c/\sqrt{\pi l_i}$, so was the crack velocity even in the steady state regime.

[30] We can illustrate this result in another way. In the steady state regime the stress intensity factor $K_t \sim \Delta P_r\sqrt{\pi\, l_c}$ was constant. The propagation being quasi-static, K_t may also be written as

$$K_t = \sqrt{G\,E}, \tag{19}$$

where G is the strain energy release rate during the steady propagation [*Lawn*, 1993] and, like K_t, stayed constant. At the onset of fissure propagation

$$K_c = \sqrt{2\,\gamma_s\,E} \sim \Delta P_r\sqrt{\pi\, l_i} = \text{constant}, \tag{20}$$

and combining equations (12), (19), and (20) we obtain

$$G \sim 2\,\gamma_s \frac{\Delta P_r}{\Delta\rho\, g\, l_i}. \tag{21}$$

Therefore the strain energy release rate G in the steady state regime was a function of γ_s and the ratio $\Delta P_r/(\Delta\rho g l_i)$. All our gelatin solids being characterized by the same surface energy γ_s, G in the steady state regime was thus determined by the ratio of the source overpressure and the buoyancy pressure in the initial fissure, that is to say by the initial source conditions.

[31] This result resembles that obtained by *Weertman* [1971a]: once the buoyancy pressure became nonnegligible and hence became the driving pressure, the length of the fissure head was determined. On the other hand, we found that the propagation was steady contrary to *Weertman* [1971b]. This difference comes from a discrepancy in his argument. Indeed, *Weertman* [1971b] assumed that the crack velocity was controlled by the fluid in the fissure, more specifically by the viscous pressure drop, but he also assumed that the crack had a constant volume. However, it is not possible to completely extract the fluid out of the crack tail as it closes. In other words, *Weertman* [1971b] took the fluid viscosity into account in the thicker part of the fissure to calculate its velocity but by assuming that the fissure could close to maintain a constant volume he implicitly neglected the viscosity in the thinner part of the fissure. In our work, we have shown that the viscosity affected only the thickness of the tail, which fed the fissure in a passive manner. The rate of propagation was seemingly entirely controlled by the fissure head and the mechanics of failure at its tip in response to its buoyancy.

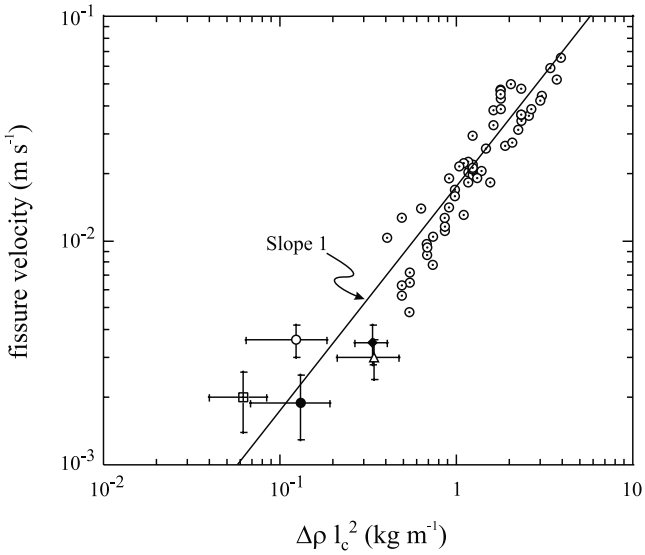

Figure 12. Fissure velocity scales with $\Delta\rho l_c^2$. Both liquid-filled fissures, same symbols as in Figure 10, and gas-driven fissures from the work of *Menand and Tait* [2001] identified by ⊙ are represented.

[32] The propagation was limited by the fracturing processes while the fissure overpressure remained constant during the initial regime. This would imply that the stress intensity factor K increased and became larger than the fracture toughness K_c:

$$K \sim \Delta P_r \sqrt{\pi\, l} \sim K_c \frac{\sqrt{l}}{\sqrt{l_i}} \geq K_c. \tag{22}$$

If this is correct, then our experimental results show that a fissure may steadily propagate in a quasi-static manner even if the stress intensity factor at its tip is greater than the fracture toughness of the solid. In our experiments K_t could be up to 4 times greater than K_c. Note however that although K apparently increased during the initial propagation regime, we observed that the fissure slowed down. This suggests that the resistance to the propagation, performed by the fracturing processes, did not stay constant but increased as the fissure propagated, and hence that fracture resistance is not a material property but is length scale dependent.

4.2. Geological Application

[33] Is it possible to apply our model to dyke propagation? Answering this question requires knowledge of the fracture resistance of rocks. Our experiments suggest that time-dependent failure of the gelatin solid controls the propagation of fissures and one can argue that mechanics of time-dependent failure might be different for gelatin and rocks. However, when applied to dyke propagation, such complex mechanics are still not well understood as time-dependent failure depends on the deformation of rocks around the dyke tip, which in turn is affected by failure of rocks at the dyke tip [*Mériaux et al.*, 1999]. On the other hand, despite that linear elastic fracture mechanics does not provide any timescale, such a framework was nevertheless successful to explain the regimes we observed in our experiments. Moreover, we have shown that gelatin behaves as an elastic, brittle solid, which is the behavior thought to be relevant for rocks, at least to leading order. We therefore think that such a framework should be entertained for dyke propagation and briefly outline the geological implications, although these should be considered as preliminary at this stage.

[34] A typical value for the fracture toughness of rocks measured in laboratory is $K_c \approx 1$ MPa m^{12} [*Atkinson*, 1984] whereas estimations deduced from field measurements are two to three orders of magnitude greater [*Delaney and Pollard*, 1981; *Reches and Fink*, 1988]. By comparing P_v and P_f we see that these two pressure scales are comparable when a dyke has a length

$$l \sim \left(\frac{K w^2}{3\sqrt{\pi}\,\eta u}\right)^{\frac{2}{3}}. \tag{23}$$

We may take for a typical mafic dyke from Hawaii a thickness $2w \sim 1$ m and a velocity $u \sim 1$ m s^{-1}. We therefore obtain that P_v and P_f are comparable when a Hawaiian dyke has a length $l \sim 60$ m if we take $K_c \approx 1$ MPa m^{12} or $l \sim 3.8$ km if we take $K_c \approx 500$ MPa m^{12}. Thus, this would suggest that, depending on the value of K_c, the resistive pressure may be the viscous pressure drop rather than the fracture pressure. However, several remarks may be made. First, the rock has to be fractured so that a dyke may propagate. If the rock has no weaknesses, in the light of the linear elastic fracture mechanics it is not possible to propagate a dyke as long as K_c has not been reached. If the rock is not fractured there is no propagation, which means $P_v \ll P_f$. Second, as previously mentioned, our experiments showed that in the case of a crack propagation initially controlled by a balance between P_e and P_f, the viscosity of the liquid acted on the propagation in a passive manner, affecting only the tail thickness. We therefore think that dyke propagation is not controlled by the viscous pressure drop but is rather controlled by the fracture resistance of the rocks. However, if rocks have weaknesses then things may be different. It has been observed that sometimes magma invades older fractures rather than propagating its own hydraulic fracture [*Delaney et al.*, 1986]. In those cases, the fracture resistance would be much lower and P_v may become the dominant resisting pressure scale. So the key question is: what is the real fracture resistance of rocks? It seems to be the key parameter for determining the propagation regime of a dyke.

4.3. Geological Implications

[35] Coupled with field measurements of dyke cross sections, our model enables us to estimate the source overpressure at the time of the emplacement of dykes and to infer whether they propagated in a steady state regime or not. We apply our model to two different magmatic systems: Hawaii and the MacKenzie Dyke Swarm, Canada. In the model framework, we have to make a number of assumptions. We first assume that the source pressure remains constant during dyke propagation. Moreover, although we are dealing with dykes that propagated toward the surface and in most cases reached it, we make the strong assumption that the surface did not have any effect on their propagation. Finally, we also assume that dykes have been

propagating in a steady state regime up to the surface. Such an assumption will be tested in order to infer the propagation regime of the dykes: if it is incompatible with the field measurements, then dykes would have been propagating in the initial transient regime.

[36] Combining equations (12) and (16), the source overpressure ΔP_r may be expressed as a function of the ratio q/u in the steady state regime:

$$\Delta P_r \sim \left[\frac{E\,(\Delta\rho\, g)^2}{2\,(1-\nu^2)\,\pi}\frac{q}{u}\right]^{\frac{1}{3}}. \qquad (24)$$

As q/u is a kinematic estimate for the fissure cross section $\pi w l$, it increases with the length of the fissure during the transient regime and is therefore greater in the steady state. Hence, substituting measured cross sections of dykes, assumed to have reached steady state propagation, into equation (24) enables us to infer a minimum value for the overpressure ΔP_r in the magmatic source that fed those dykes. Moreover, equation (16) enables us to estimate the transition height between the transient and steady state regimes from the measurements of these dyke cross sections. Figure 13 represents the dyke cross section as a function of the source overpressure (equation (24)) and of the critical height for the transition between regimes (equation (16)), we use E = 40 GPa, ν = 0.25 and $\Delta\rho$ = 300 kg m^{-3} as typical values for the Earth's crust and for the density contrast between rock and magma. Typical cross sections for dykes from Hawaii and the MacKenzie Dyke Swarm, shown as ellipses, have been drawn as well. Table 2 gives the estimations of dyke cross sections, source overpressures and transition heights (equations (16) and (24)) for Hawaii and the MacKenzie Dyke Swarm.

[37] The magma chamber in Hawaii is thought to be about 1.5 km below the surface [*Ryan et al.*, 1981; *Rubin and Pollard*, 1987]. This depth is comparable to our transition height estimation. However, our density contrast may be an overestimation for that between magma and rocks close to the surface. This would increase the transition height and thus suggests that Hawaiian dykes fed by shallow regions of the magma chamber may be unlikely to attain the steady state regime. Equation (24) estimates the source overpressure to be between about 40 and 100 bars. These values are close to those given by *Rubin and Pollard* [1987]. However, an overestimation of the density contrast would also lead to an underestimated source overpressure suggesting that ΔP_r would therefore be greater than 100 bars.

[38] In the Canadian shield, the MacKenzie Dyke Swarm is more than 2000 km long and 500 km wide with a mean dyke thickness of 30 m. It is thought to appear 1.27 Ga ago because of a giant mantellic plume [*Fahrig*, 1987; *LeCheminant and Heaman*, 1989] the head of which would have measured 1000 km in diameter [*Ernst and Baragar*, 1992]. According to *Ernst and Baragar* [1992] the flow in dykes was vertical above the plume head and horizontal around it. Although such a plume would have strongly thinned the lithosphere, this thinning remains unknown and a comparison with our transition height estimation is therefore difficult. However, the presence of sills [*LeCheminant and Heaman*, 1989] as well as the indication of horizontal flow [*Ernst and Baragar*, 1992] suggest that the propagation was dominated by the overpressure in the plume head rather than by the buoyancy of the magma. Vertical dykes would have therefore propagated in a non-steady state regime and our estimations of transition height and source overpressure would be underestimated. This would suggest an enormous overpressure in the plume head, more than 1500 bars, at the time of the swarm emplacement. If we have overestimated dyke cross sections, because we considered dykes that propagated laterally and not vertically, our model would still predict overpressures of several hundreds of bars. Another possibility is that a giant mantellic plume such as this one would have dramatically modified the thermal structure of the lithosphere and, as a result, its stiffness would have been strongly reduced. In that case, our estimated source overpressure would be lowered.

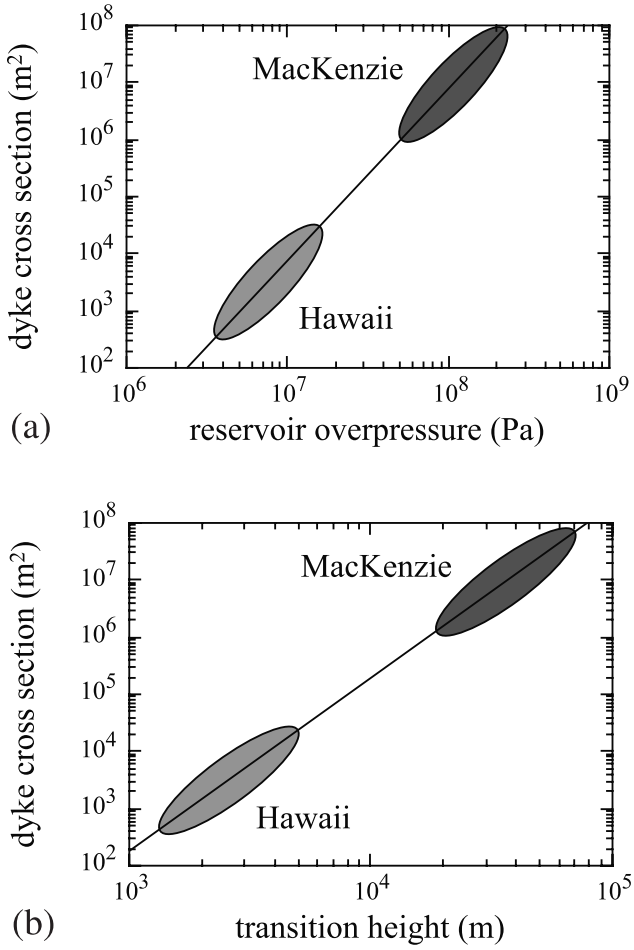

Figure 13. Dyke cross section as a function of (a) source overpressure (equation (24)) and (b) transition height (equation (16)). E = 40 GPa, ν = 0.25, and $\Delta\rho$ = 300 kg m^{-3}. Ellipses are estimations of typical dyke cross sections estimated for Hawaii and MacKenzie Dyke Swarm.

[39] Are such overpressures realistic? We have assumed that dyke initiation and propagation are controlled by the fracture toughness of rocks, which is thought to be independent of the dimensions of the dykes as well as their loading. This seems to be in contradiction with our results that suggest a greater source overpressure is needed to create a greater geological object, such as a giant dyke swarm, and therefore that fracturing processes depend on a length scale.

Table 2. Source Overpressures and Transition Heights Between Regimes Estimated for Hawaii and the MacKenzie Dyke Swarm

Parameter	Hawaii	MacKenzie
Dyke cross section (m^2)	10^3–10^4	3×10^6–3×10^7
Source overpressure (bar)	40–80	600–1200
Transition height (km)	1–3	20–40

The source overpressures and transition heights have been estimated using equations (24) and (16), respectively.

However, fracture toughness estimated from field measurements are 10^2–10^3 greater than those measured in laboratory on rock samples [*Delaney and Pollard*, 1981; *Atkinson*, 1984; *Reches and Fink*, 1988] and it has been argued that the fracture energy required to propagate a dyke, or measured for earthquakes, is many orders of magnitude larger than laboratory-scale measurements [*Rudnicki*, 1980; *Delaney et al.*, 1986]. Both field and laboratory observations can only really be consistent if fracture toughness is scale dependent. Indeed, it has been argued that rock fracture toughness does scale with the size of the fracture because the volume of rock affected, and hence undergoing damage, is greater [*King*, 1983; *Scholtz et al.*, 1993]. Increase in the resistance to propagation of a fault with the length of the fault can explain why small earthquakes occur; if this were not the case, earthquakes would always propagate unstably and therefore become "megaearthquakes." In short, damage and fracture at one scale lead not to catastrophic failure of the rock (as happens in small-scale experiments on rock samples) but to damage and fracture at larger scales in a process of evolving damage [*King and Sammis*, 1992]. It therefore seems that the fracture dominated regime, which we observed in our experiments and in which a dissipative, scale-dependent process resists fissure propagation, is likely to exist under geological conditions.

5. Conclusion

[40] Fissure propagation from a reservoir with constant overpressure is characterized by two regimes. Initially, the propagation is controlled by a balance between the source pressure and the fracture pressure. In this transient regime both the injection rate and the fissure velocity depend on the initial conditions. Once the buoyancy pressure overcomes the source pressure, a steady state is achieved. The fissure develops a bulbous head, in which buoyancy pressure balances the fracture pressure that resists the propagation, fed by a thinner tail, the thickness of which is determined by a balance between buoyancy and viscous pressure gradient. Fissure velocity and injection rate become constant at the transition between regimes. Even in the steady state regime, the velocity and the injection rate reflect the source conditions because the fissure latches onto a steady state regime that is consistent with the source characteristics. Likewise, the strain energy release rate during the steady propagation is determined by the initial source conditions.

[41] Although our model cannot, at this preliminary stage, predict the propagation velocity of a liquid-filled fissure, it does nevertheless provide constraints on the failure mechanism: the steady propagation velocity appears to be proportional to the square of the height of the buoyant fissure head. Moreover, the fissure can propagate steadily even though the stress intensity factor at its tip is greater than the fracture toughness of the host solid.

[42] Our model suggests that the cross-sectional area of dykes provides two quantitative pieces of information. It first gives the nature of the propagation regime of the dykes, whether it is steady or not. Second, it gives an estimation of the overpressure present in the source at the time of their emplacement. These overpressures appear to depend on the dimensions of the dykes, suggesting a length scale dependence of time-dependent failure of rocks. Hence, like fault propagation, dyke propagation seems very likely to be controlled by the fracture resistance of rocks.

[43] **Acknowledgments.** We thank Claude Jaupart, Geoffrey King, and Allan Rubin for fruitful discussions. Reviews by Amotz Agnon and John Lister have greatly improved the manuscript. We also thank Gérard Bienfait for help with experiments.

References

Atkinson, B. K., Subcritical crack growth in geological materials, *J. Geophys. Res.*, *89*, 4077–4114, 1984.

Barenblatt, G. I., The mathematical theory of equilibrium cracks in brittle fracture, *Adv. Appl. Mech.*, *7*, 55–129, 1962.

Brandsdóttir, B., and P. Einarsson, Seismic activity associated with the September 1977 deflation of the Krafla central volcano in northeastern Iceland, *J. Volcanol. Geotherm. Res.*, *6*, 197–212, 1979.

Delaney, P. T., and D. D. Pollard, Deformation of host rocks and flow of magma during growth of Minette dikes and breccia-bearing intrusions near Ship Rock, New Mexico, *U. S. Geol. Surv. Prof. Pap.*, *1202*, 61 pp., 1981.

Delaney, P. T., D. D. Pollard, J. L. Ziony, and E. H. McKee, Field relations between dikes and joints: Emplacement processes and paleostress analysis, *J. Geophys. Res.*, *91*, 4920–4938, 1986.

Einarsson, P., and B. Brandsdóttir, Seismological evidence for lateral magma intrusion during the July 1978 deflation of the Krafla volcano in NE-Iceland, *J. Geophys.*, *47*, 160–165, 1980.

Emerman, S. H., D. L. Turcotte, and D. A. Spence, Transport of magma and hydrothermal solutions by laminar and turbulent fluid fracture, *Phys. Earth Planet. Inter.*, *41*, 249–259, 1986.

Ernst, R. E., and W. B. A. Baragar, Evidence from magnetic fabric for the flow pattern of magma in the MacKenzie giant radiating dyke swarm, *Nature*, *356*, 511–513, 1992.

Fahrig, W. F., The tectonic settings of continental mafic dyke swarms: Failed arm and early passive margin, in *Mafic Dyke Swarms*, edited by H. C. Halls and W. F. Fahrig, pp. 331–348, Geol. Assoc. of Can., St. Johns, Newfoundland, 1987.

Fiske, R. S., and E. D. Jackson, Orientation and growth of Hawaiian volcanic rifts: The effect of regional structure and gravitational stresses, *Proc. R. Soc. London*, *329*, 299–326, 1972.

Griffith, A. A., The phenomena of rupture and flow in solids, *Philos. Trans. R. Soc. London, Ser. A*, *221*, 163–198, 1920.

Heimpel, M., and P. Olson, Buoyancy-driven fracture and magma transport through the lithosphere: Models and experiments, in *Magmatic Systems*, edited by M. P. Ryan, pp. 223–240, Academic, San Diego, Calif., 1994.

Hyndman, D. W., and D. Alt, Radial dikes, laccoliths and gelatin models, *J. Geol.*, *95*, 763–774, 1987.

Irwin, G. R., Analysis of stresses and strains near the end of a crack traversing a plate, *J. Appl. Mech.*, *24*, 361–364, 1957.

King, G. C. P., The accommodation of large strains in the upper lithosphere of the Earth and other solids by self-similar faults systems: The geometrical origin of b-value, *Pure Appl. Geophys.*, *121*, 761–815, 1983.

King, G. C. P., and C. Sammis, The mechanisms of finite brittle strain, *Pure Appl. Geophys.*, *138*, 611–640, 1992.

Lawn, B., *Fracture of Brittle Solids* (*Second Edition*), 398 pp., Cambridge Univ. Press, New York, 1993.

LeCheminant, A. N., and L. M. Heaman, Mackenzie igneous events, Canada: Middle Proterozoic hotspot magmatism associated with ocean spreading, *Earth Planet. Sci. Lett.*, *96*, 38–48, 1989.

Lister, J. R., Buoyancy-driven fluid fracture: The effects of material toughness and of low-viscosity precursors, *J. Fluid Mech.*, *210*, 263–280, 1990a.

Lister, J. R., Buoyancy-driven fluid fracture: Similarity solutions for the horizontal and vertical propagation of fluid-filled cracks, *J. Fluid Mech.*, *217*, 213–239, 1990b.

Lister, J. R., and R. C. Kerr, Fluid-mechanical models of crack propagation and their application to magma transport in dykes, *J. Geophys. Res.*, *96*, 10,049–10,077, 1991.

Maaløe, S., The generation and shape of feeder dykes from mantle sources, *Contrib. Mineral. Petrol.*, *96*, 47–55, 1987.

McGuire, W. J., and A. D. Pullen, Location and orientation of eruptive fissures and feeder-dykes at Mount Etna: Influence of gravitational and regional tectonic stress regimes, *J. Volcanol. Geotherm. Res.*, *38*, 325–344, 1989.

Menand, T., and S. R. Tait, A phenomenological model for precursor volcanic eruptions, *Nature*, *411*, 678–680, 2001.

Mériaux, C., and C. Jaupart, Dike propagation through an elastic plate, *J. Geophys. Res.*, *103*, 18,295–18,314, 1998.

Mériaux, C., J. R. Lister, V. Lyakhovsky, and A. Agnon, Dyke propagation with distributed damage of the host rock, *Earth Planet. Sci. Lett.*, *165*, 177–185, 1999.

Pollard, D. D., Derivation and evaluation of a mechanical model for sheet intrusion, *Tectonophysics*, *19*, 233–269, 1973.

Pollard, D. D., Elementary fracture mechanics applied to the structural interpretation of dykes, in *Mafic Dyke Swarms*, edited by H. C. Halls and W. F. Fahrig, pp. 5–24, Geol. Assoc. of Can., St. Johns, Newfoundland, 1987.

Pollard, D. D., and A. M. Johnson, Mechanics of growth of some laccolithic intrusions in the Henry Mountains, Utah, II, Bending and failure of overburden layers and sills formation, *Tectonophysics*, *18*, 311–354, 1973.

Reches, Z., and J. Fink, The mechanism of intrusion of the Inyo Dike, Long Valley Caldera, California, *J. Geophys. Res.*, *93*, 4321–4334, 1988.

Rubin, A. M., Tensile fracture of rocks at high confining pressure: Implications for dyke propagation, *J. Geophys. Res.*, *98*, 15,919–15,935, 1993a.

Rubin, A. M., Dikes vs. diapirs in viscoelastic rock, *Earth Planet. Sci. Lett.*, *119*, 641–659, 1993b.

Rubin, A. M., Getting granite dikes out of the source region, *J. Geophys. Res.*, *100*, 5911–5929, 1995a.

Rubin, A. M., Propagation of magma-filled cracks, *Annu. Rev. Earth Planet. Sci.*, *23*, 287–336, 1995b.

Rubin, A. M., and D. D. Pollard, Origin of blade-like dikes in volcanic rift zones, *U. S. Geol. Surv. Prof. Pap.*, *1350*, 1449–1470, 1987.

Rudnicki, J. W., Fracture mechanics applied to the Earth's crust, *Annu. Rev. Earth Planet. Sci.*, *8*, 489–525, 1980.

Ryan, M. P., R. Y. Koyanagi, and R. S. Fiske, Modeling the three-dimensional structure of macroscopic magma transport systems: Application to Kilauea volcano, Hawaii, *J. Geophys. Res.*, *86*, 7111–7129, 1981.

Scholtz, C. H., N. H. Dawers, J.-Z. Yu, M. H. Anders, and P. A. Cowie, Fault growth and fault scaling laws: Preliminary results, *J. Geophys. Res.*, *98*, 21,951–21,961, 1993.

Sneddon, I. N., The distribution of stress in the neighborhood of a crack in an elastic solid, *Proc. R. Soc. London*, *187*, 229–260, 1946.

Sneddon, I. N., and S. C. Das, The stress intensity factor at the tip of an edge crack in an elastic half-plane, *Int. J. Eng. Sci.*, *9*, 25–36, 1971.

Spence, D. A., and P. Sharp, Self-similar solutions for elastohydrodynamic cavity flow, *Proc. R. Soc. London, Ser. A*, *400*, 289–313, 1985.

Spence, D. A., and D. L. Turcotte, Magma-driven propagation of cracks, *J. Geophys. Res.*, *90*, 575–580, 1985.

Spence, D. A., and D. L. Turcotte, Buoyancy-driven magma fracture: A mechanism for ascent through the lithosphere and the emplacement of diamonds, *J. Geophys. Res.*, *95*, 5133–5139, 1990.

Spence, D. A., P. W. Sharp, and D. L. Turcotte, Buoyancy-driven crack propagation: A mechanism for magma migration, *J. Fluid Mech.*, *174*, 135–153, 1987.

Takada, A., Experiments study on propagation of liquid-filled crack in gelatin: Shape and velocity in hydrostatic stress condition, *J. Geophys. Res.*, *95*, 8471–8481, 1990.

Timoshenko, S. P., and J. N. Goodier, *Theory of Elasticity* (*Third Edition*), 567 pp., McGraw-Hill, New York, 1970.

Weertman, J., Theory of water-filled crevasses in glaciers applied to vertical magma transport beneath oceanic ridges, *J. Geophys. Res.*, *76*, 1171–1183, 1971a.

Weertman, J., Velocity at which liquid-filled cracks move in the Earth's crust or in glaciers, *J. Geophys. Res.*, *76*, 8544–8553, 1971b.

White, F. M., *Viscous Fluid Flow*, 725 pp., McGraw-Hill, New York, 1974.

T. Menand, BP Institute for Multiphase Flow, University of Cambridge, Madingley Rise, Madingley Road, Cambridge CB3 0EZ, UK. (thierry@bpi.cam.ac.uk)

S. R. Tait, Department of Earth Sciences and Engineering, Imperial College of Science, Technology and Medicine, RSM Building, Prince Consort Road, London SW7 2BP, UK. (steve.tait@ic.ac.uk)